

Supporting Information

Quantitative characterization of conformational-specific protein-DNA binding using a dual-spectral interferometric imaging biosensor

Xirui Zhang[†], George G. Daaboul^{†,‡}, Philipp S. Spuhler[†], Peter Dröge[§], and M. Selim Ünlü^{†,‡,}*

[†]Department of Biomedical Engineering, Boston University, Boston, Massachusetts, 02215, United States, [‡]Department of Electrical and Computer Engineering, Boston University, Boston, Massachusetts, 02215, United States, and [§]School of Biological Sciences, Nanyang Technological University, Singapore 637551

KEYWORDS: DNA bending, protein-DNA interactions, integration host factor, optical biosensor, DNA conformation, fluorescence vertical sectioning, DNA microarray

*Corresponding author: selim@bu.edu

Contents

1. DNA sequences and nomenclature (Table 1S).
2. SDS-PAGE assay of IHF stock solution (Figure 1S).
3. Determination of the concentration of IHF stock solution by Bradford assay (Figure 2S).
4. Calculation of dissociation constants (Figure 3S, Figure 4S; Table 2S).
5. Geometric model for quantification of DNA bending angle induced by specific IHF binding (Figure 4S).
6. Customized flow cell assembly (Figure 5S).
7. Real-time measurement of average fluorophore height change by SSFM (Figure 6S).
8. Summary of binding parameters obtained from additive isotherm model fitting (Table 3S).
9. Average surface densities of 10 dsDNA spots and bound IHF at equilibrium (Table 4S).
10. Effects of surface densities on the binding and bending of dsDNA (Tables 5S and 6S, Figures 7S-10S).
11. References.

1. DNA sequences

Table 1S. 60-bp DNA sequences and nomenclature.

Name	DNA sequences
H'(34)	NH ₂ -C6-5'-GCT GTT AGA AGA TAG GGC CAA AAA AGC ATT GCT TAT CAA TTT GTT GCA CCT GAC CGA TGA-3'
Complement	5'-Atto647N-TCA TCG GTC AGG TGC AAC AAA TTG ATA AGC AAT GCT TTT TTG GCC CTA TCT TCT AAC AGC-3'
H'(36)	NH ₂ -C6-5'-GAG CTG TTA GAA GAT AGG GCC AAA AAA GCA TTG CTT ATC AAT TTG TTG CAC CTG ACC GAT-3'
Complement	5'-Atto647N-ATC GGT CAG GTG CAA CAA ATT GAT AAG CAA TGC TTT TTT GGC CCT ATC TTC TAA CAG CTC-3'
H'(39)	NH ₂ -C6-5'-GCT CTG AGA AGA CAG TGA CCG GCC AAA AAA GCA TTG CTT ATC AAT TTG TTG CAC CTG ACC-3'
Complement	5'-Atto647N-GGT CAG GTG CAA CAA ATT GAT AAG CAA TGC TTT TTT GGC CGG TCA CTG TCT TCT CAG AGC-3'
H'(34)A	NH ₂ -C6-5'-GCT GTT AGA AGA TAG GGC CAA AAA AGC ATT GCT TAT CAA TTT GTA GCA CCT GAC CGA TGA-3'
Complement	5'-Atto647N-TCA TCG GTC AGG TGC TAC AAA TTG ATA AGC AAT GCT TTT TTG GCC CTA TCT TCT AAC AGC-3'
H'(34)Proximal	5'-GCT GTT AGA AGA TAG GGC CAA AAA AGC ATT GCT TAT CAA TTT GTT GCA CCT GAC CGA TGA-3'-C6-NH ₂
Complement	5'-Atto647N-TCA TCG GTC AGG TGC AAC AAA TTG ATA AGC AAT GCT TTT TTG GCC CTA TCT TCT AAC AGC-3'
Control	NH ₂ -C6-5'-CAA CAG CCC CGC TCT AGT TTG GGT TCA TAT ATC GGG ACA GGC CTC GGA ATC AAG TGC ATG-3'
Complement	5'-Atto647N-CAT GCA CTT GAT TCC GAG GCC TGT CCC GAT ATA TGA ACC CAA ACT AGA GCG GGG CTG TTG-3'

The amine groups on the 5' end of the first strand of the IHF-binding sequences and the control sequence covalently bind to the functional groups on the polymer-functionalized surface of the biosensor substrate. We chose to use Atto647N fluorophores as fluorescence labels for the dsDNA molecules in the experiments. After hybridization, the Atto647N fluorophores tagged to the 5' end of the complementary sequences reside on the surface-distal end of the double-stranded DNA. The IHF-binding sequence H'(34) Proximal has its amine group modified at the 3' end so that after hybridization, the Atto647N fluorophores reside on the surface-proximal end of the double-stranded DNA after hybridization. The axial height difference between the surface-proximal and surface-distal end fluorophores is used for calculation of dsDNA orientation. Also, the surface-proximal fluorophores provides a baseline for measurement of the axial height changes of surface-distal fluorophores resulted from IHF binding.

2. SDS-PAGE assay

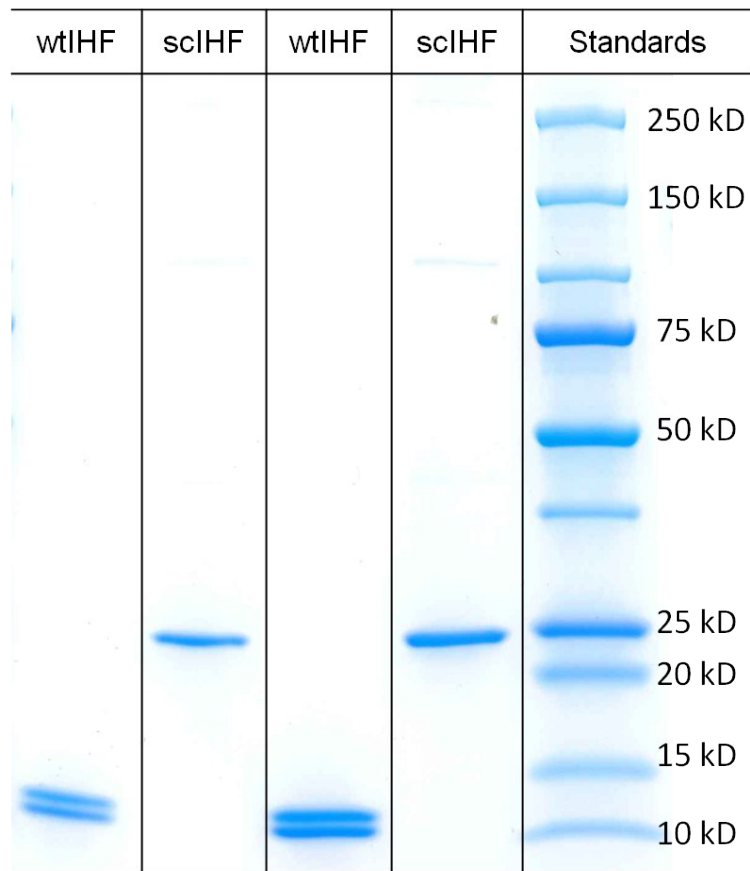


Figure 1S. Denaturing SDS-PAGE assay to check the integrity of IHF proteins after shipment. Wild-type IHF (wtIHF) contains two subunits or amino acid chains and appears as two bands. Engineered single-chain IHF (scIHF) contains one amino acid chain and appears as one band.

3. Determination of the concentration of IHF stock solution by Bradford assay

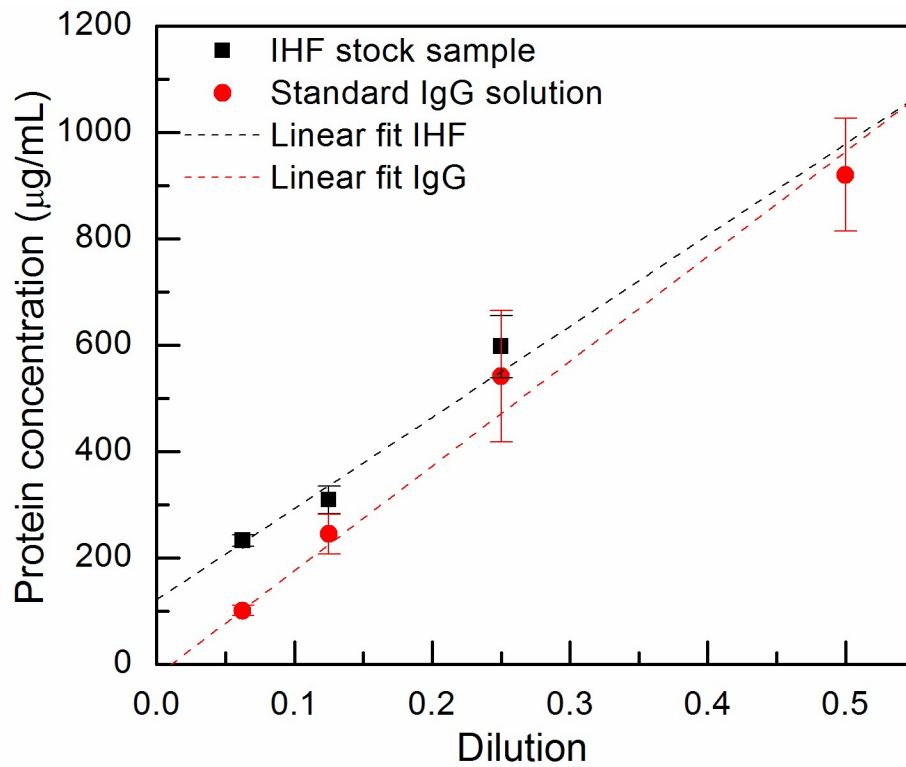


Figure 2S. Determine the concentration of IHF stock solution by Bradford assay. Two dilutions of standard IgG solution were prepared. One IgG dilution was used to generate the standard calibration curve, and the other was measured as a Control sample in the same way as IHF stock sample dilutions. The concentration of the stock IHF solution was determined to be 83.2 μM from the assay.

4. Calculation of dissociation constants

In the case of IHF to DNA molecular binding ratio measured by WLRS, the equation for the adapted Langmuir binding isotherm is:

$$\langle R \rangle = \langle R_{\max} \rangle \frac{x}{K_d + x},$$

where $\langle R \rangle$ is the measured average IHF to DNA binding ratio, x is the IHF concentration, K_d is the dissociation constant of IHF binding to the DNA sequence, and $\langle R_{\max} \rangle$ is the maximum IHF to DNA ratio at equilibrium. In the case of average fluorophore height change measured by SSFM, the equation for the adapted Langmuir binding isotherm is:

$$\langle \Delta h \rangle = \langle \Delta h_{\max} \rangle \frac{x}{K_d + x},$$

where $\langle \Delta h \rangle$ is the measured average fluorophore height change, x is the IHF concentration, K_d is the dissociation constant of IHF binding to the DNA sequence, and $\langle \Delta h_{\max} \rangle$ is the maximum average fluorophore height change at equilibrium.

At first, we obtained the K_d of IHF to the IHF-binding sequence H'(39) as 6.7 nM from measurements of the IHF to DNA binding ratios shown in Figure 2(a) while as 0.7 nM from measurements of surface-distal fluorophore height changes shown in Figure 2(b). Both K_d measurements fall in the typical range 0.5 to 20 nM of the dissociation constant of IHF binding to the 34-bp H' consensus sequence^{1,2}.

Since the fluorophore height changes measured by SSFM and the IHF to DNA binding ratios measured by WLRS were simultaneous measurements of the same binding assay, we initially expect the two equilibrium isotherms to generate similar K_d values. However, as discussed in the main text, the two equilibrium isotherms are different. When we fit both isotherms to the

same adapted Langmuir binding isotherm model, we found that the K_d value from WLRS measurements was about 10 times of that from SSFM measurements. This discrepancy of the K_d value between the fluorophore height change measurement and the IHF to DNA binding ratio measurement was consistent across the four DNA sequences containing the consensus H' binding site (See Table 2S below).

Table 2S. Discrepancy of the $K_{d(specific)}$ value between the fluorophore height change measurement by SSFM and the IHF to DNA binding ratio measurement by WLRS.

$K_{d(specific)}$	H'(23)	H'(34)	H'(36)	H'(34)A
SSFM	1.1±0.1	0.7±0.1	0.6±0.1	1.8±0.2
WLRS	10.6±2.4	7.1±2.0	5.4±1.3	4.5±1.7

Since IHF have both specific and nonspecific binding modes, we hypothesize that the IHF to DNA binding ratios measured by WLRS were contributed by both specific binding and nonspecific binding of IHF whereas the fluorophore height changes measured by SSFM were only contributed by conformation changes of dsDNA due to specific binding of IHF. We thus propose a generalized additive Langmuir binding isotherm model to decouple the specific and non-specific binding modes of IHF to DNA measured by WLRS. The additive model simply adds two adapted Langmuir binding isotherms, one describing specific binding of IHF to DNA, the other describing nonspecific binding of IHF to DNA:

$$\langle R \rangle = \langle R_{specific} \rangle \frac{x}{K_{d(specific)} + x} + \langle R_{nonspecific} \rangle \frac{x}{K_{d(nonspecific)} + x}$$

where $\langle R \rangle$ is the measured average IHF to DNA binding ratio, x is the IHF concentration in binding buffer solution, $K_{d(specific)}$ is the dissociation constant of specific IHF binding to the DNA sequence, $K_{d(nonspecific)}$ the dissociation constant of nonspecific IHF binding to the DNA sequence, $\langle R_{specific} \rangle$ is the maximum average ratio of IHF specifically bound to DNA at

equilibrium, and $\langle R_{nonspecific} \rangle$ is the maximum average ratio of IHF nonspecifically bound to DNA at equilibrium.

We further assume that the K_d obtained from the equilibrium binding isotherm of fluorophore height changes resulted from DNA bending characterizes conformational specific binding of IHF to DNA and is thus designated as $K_{d(specific)}$. This assumption is validated based on the low fluorophore height change measurements of the nonspecific Control sequence, which showed minimum DNA bending (Figure 2(b)). Nonlinear Least Square Fitting was used to fit the equilibrium isotherm of the average IHF to DNA binding ratio to the additive model. The three fitting parameters obtained are $\langle R_{specific} \rangle$, $\langle R_{nonspecific} \rangle$, and $K_{d(nonspecific)}$. We compare the fitting curves of the equilibrium isotherm of the average IHF to DNA binding ratio based on the adapted Langmuir binding isotherm model shown in Figure 3(a) to that based on the additive model shown in **Figure 3S(b)**. Not only can we visibly see that the additive model better describes the equilibrium isotherm of the average IHF to DNA binding ratio, but we can also use quantitative criteria to compare the two fitting curves, such as the adjusted R^2 , which penalizes addition of new variables in the fitting and is shown together with the fitting curves. The adjusted R^2 of the additive model fitting, albeit penalized for added fitting variables, is larger than that of the adapted Langmuir isotherm model, demonstrating that the additive model better describes our equilibrium measurements of IHF to DNA binding ratios (**Figure 3S**). Fitting the Control sequence to the additive model obtained an average specific binding ratio of 0.05 and an average nonspecific binding ratio of 2.6, same as the average IHF to DNA binding ratio of the Control sequence obtained from the single Langmuir binding isotherm fit. This demonstrates that the Control sequence only has one mode of binding, nonspecific binding. Therefore, we resort to the additive Langmuir binding isotherm model to understand the measurements of average IHF

to DNA binding ratio and continue to use the adapted Langmuir binding isotherm to characterize the measurements of average fluorophore height change of IHF-binding sequences.

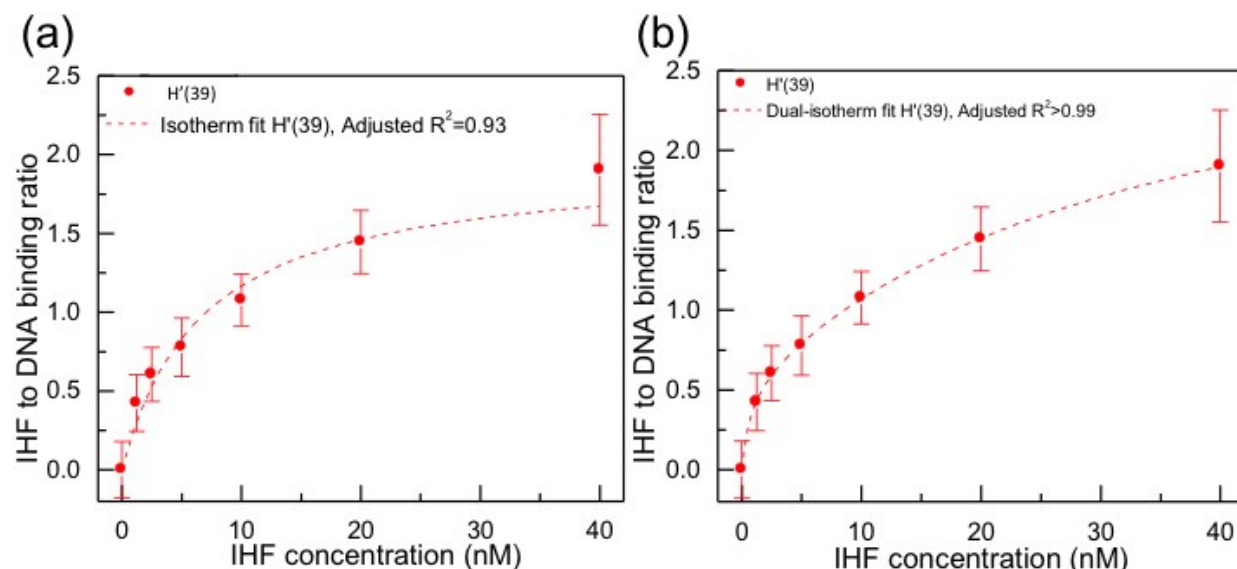


Figure 3S. The additive model comprising contributions from both specific and nonspecific binding better describes IHF to DNA binding ratio measurements at equilibrium. (a) Equilibrium binding isotherm fitting of average IHF to DNA binding ratios using a single Langmuir binding isotherm model. (b) Equilibrium binding isotherm fitting of average IHF to DNA binding ratios using the additive Langmuir binding isotherm model proposed in the main text.

5. Geometric model for quantification of DNA bending angle induced by specific IHF binding

The persistence length of dsDNA molecule is approximately 50 nm or 150-bp, and previous studies have shown that 60-bp dsDNA molecules, much shorter than the persistence length, can be modeled as rigid rods when immobilized on a surface³⁻⁶. The orientation, length, surface density of the rigid rod-like dsDNA molecules and the location of the IHF consensus binding sequence along the dsDNA affect the measured fluorophore height change (**Figure 4S**). The average orientation of the dsDNA to the surface can be obtained by trigonometric calculations using the measured average height difference between the surface-distal and surface-proximal fluorophores (not shown in data) and root-mean-square end-to-end distance of the dsDNA before IHF binding⁶.

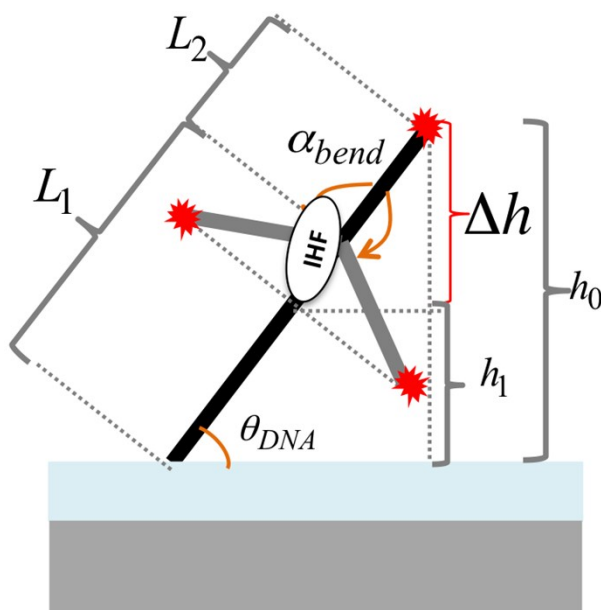


Figure 4S. Schematic illustration of geometrical calculation of dsDNA bending angle induced by IHF binding.

Since SSFM measures ensemble average within a focused region, the measured average of fluorophore height change after IHF binding includes both specifically bent and unbent dsDNA molecules within the region. Now that we can obtain average IHF to DNA specific binding ratio of the same focused region from the simultaneous WLRS measurement, we can use the average IHF to DNA specific binding ratio to normalize ensemble average of fluorophore height changes. Therefore, we then obtain the average fluorophore height change of just the bent dsDNA molecules for calculation of the DNA bending angle. We thus propose a geometric model to calculate the average bending angle of dsDNA induced by specific IHF binding using the average fluorophore height changes measured by SSFM.

First, we define a few parameters for the calculation of the dsDNA bending angle. We designate $\langle \Delta h_{measured} \rangle$ as the measured average fluorophore height change by SSFM, $\langle \Delta h \rangle$ as the average fluorophore height change of dsDNA molecules specifically bound to IHF, $\langle h_0 \rangle$ as the initial average height difference between dsDNA surface-distal and surface-proximal ends, $\langle R_{specific} \rangle$ as the average IHF to DNA specific binding ratio obtained from WLRS measurements, θ_{DNA} as the orientation of one dsDNA molecule to the surface while $\langle \theta_{DNA} \rangle$ as the average orientation of dsDNA molecules to the surface in the focused region, and P as the nucleotide position of the center of the binding sequence from the first nucleotide of the DNA sequence attached to the surface (**Figure 4S**). The distance between nucleotides of B-form DNA is 0.34 nm, so for 60-bp long dsDNA, we have:

$$L_1 = (P-1) \times 0.34, L_2 = (60-P-1) \times 0.34.$$

The average height of surface-distal end of bent dsDNA molecules is designated as $\langle h_1 \rangle$, a geometric average given that the DNA can have various bending directions. Thus we can give the relationship between the measured ensemble average of the fluorophore height change of all dsDNA molecules and that of dsDNA molecules specifically bound to IHF by:

$$\langle \Delta h_{measured} \rangle = \langle h_0 \rangle - ((1 - R_{specific}) \cdot \langle h_0 \rangle + R_{specific} \cdot \langle h_1 \rangle) = R_{specific} \cdot (\langle h_0 \rangle - \langle h_1 \rangle) = R_{specific} \cdot \langle \Delta h \rangle$$

Based on geometric calculation, for each dsDNA molecule, we have:

$$\Delta h = (L_2 + L_2 \cdot \sin(\alpha_{bend} - 90^\circ)) \cdot \sin \theta_{DNA}.$$

Thus the average bending angle $\langle \alpha_{bend} \rangle$ of dsDNA molecules specifically bound to IHF is:

$$\langle \alpha_{bend} \rangle = \arcsin\left(\left(\frac{\langle \Delta h_{measured} \rangle}{\langle R_{specific} \rangle \cdot \langle \theta_{DNA} \rangle} - L_2\right) / L_2\right) + 90^\circ.$$

Here we note that in this geometric model, $\langle \Delta h_{measured} \rangle$, $\langle h_0 \rangle$, $\langle h_1 \rangle$, $\langle \Delta h \rangle$, $\langle \theta_{DNA} \rangle$, and $\langle R_{specific} \rangle$ are ensemble average values, and h_0 , h_1 , Δh , θ_{DNA} , P , L_1 , and L_2 are geometric parameters of each individual DNA molecule in the model (**Figure 4S**).

The statistical average of $\langle \theta_{DNA} \rangle$ was approximated by calculated average DNA orientation from $\langle h_0 \rangle$:

$$\langle \theta_{DNA} \rangle = \arcsin\left(\langle h_0 \rangle / \sqrt{\langle r^2 \rangle}\right)$$

where $\sqrt{\langle r^2 \rangle}$ is the root-mean-square (rms) end-to-end distance of the dsDNA based on the worm-like chain model^{5,7}

We calculated the average bending angle of DNA sequence H'(39) caused by IHF specific binding as 162.4° with a standard deviation of 11.3°. Since we need to use the fitted variables, the mean and standard errors of the variables were used to calculate the estimated average of the bending angle and its standard deviation. The measured average DNA bending angle agrees with the DNA bending angles measured by other methods, such as gel electrophoresis and X-ray crystallography⁸, which range from 120° to 180°. Our result demonstrates that the simultaneous detection of IHF-DNA interaction by combining WLRS and SSFM can accurately and conveniently determine the DNA bending angle caused by specific IHF binding.

6. Customized flow cell assembly

All measurements were made on substrates fixed in the flow cell as described below in Figure 5S. The height of the flow cell is 1 mm, the length of the flow cell is 20 mm, and the width of the flow cell is 5 mm. In dry measurements, the substrate resided in air in the flow cell. In wet measurements, such as all the DNA conformation and IHF binding measurements, the chip was immersed in buffer solution. Each buffer solution was driven by a peristaltic pump into and out of flow cell through the inlet and outlet via stainless steel and non-shedding silicon tubing and tubing connectors.

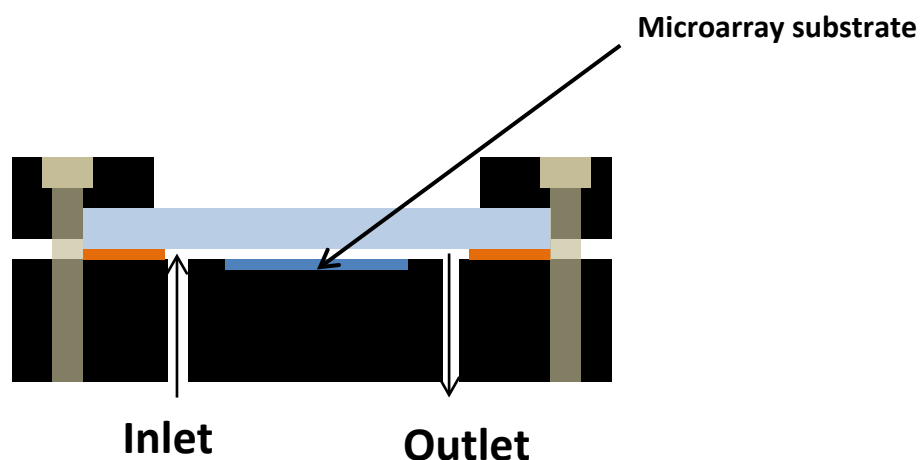


Figure 5S. Schematic illustration of customized flow cell assembly.

7. Real-time measurement of average fluorophore height change by SSFM

We performed two real-time experiments to estimate the time for IHF to surface-immobilized DNA binding to reach equilibrium in our customized flow cell. In two separate experiments, we measured fluorophore height change 60-bp DNA sequence H'(39) binding to 40 nM IHF solution with either low salt (50 mM NaCl) or high salt concentration (150 mM NaCl). As shown in Figure 6S below, average fluorophore height change of 7 DNA spots reached equilibrium after approximately 15 minutes of incubation in both high salt buffer and low salt buffer.

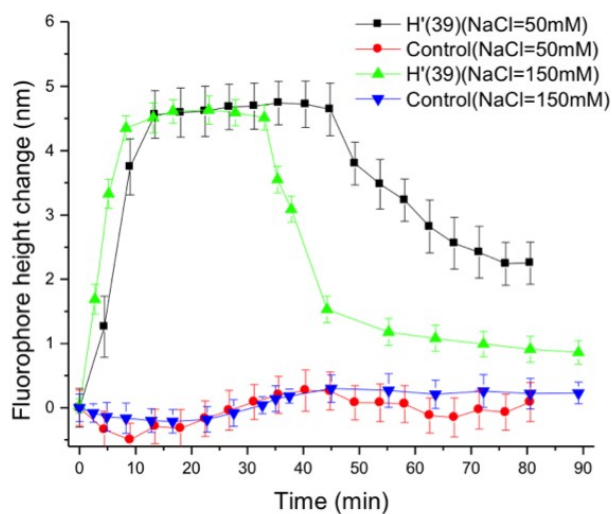


Figure 6S. Real-time measurement of fluorophore height change of DNA sequence H'(39) induced by IHF binding buffer containing with 50 mM NaCl or 150 mM NaCl.

Because the design of the customized flow cell was not optimized, IHF-dsDNA binding took place in a diffusion-limited or mass transport-limited regime⁹. In our current flow cell setup, as shown in Figure 6S, a typical period of time for the binding to reach equilibrium ranges from about 10 minutes to about 30 minutes.

The period of time required for the binding reaction to reach equilibrium in the customized flow cell is determined by various factors, such as the concentration, binding constants, and diffusivity of IHF, the dimensions of the flow cell, the concentration of IHF, and the flow rate of the binding solution. These factors can be designed and optimized to reduce the time required to reach equilibrium, such as increasing the concentration of IHF or reducing the height of the flow cell. Accordingly, future efforts can be made to optimize the flow cell design to operate in a reaction-limited regime by reducing the height of the flow cell or introducing mixing or turbulence in the flow cell. Then, the limit of our imaging biosensor platform for dynamic measurements will be the integration time required for obtaining the fluorescence spectrums, which ranges from 0.1 second to 1 second using the current optical setup.

8. Summary of binding parameters obtained from dual isotherm model fitting

Table 3S. Binding parameters \pm Standard Error (SE) for each DNA sequence.

DNA Sequence	$\langle \Delta h_{max} \rangle$ (nm)	$\langle R_{specific} \rangle$	$K_{d(specific)}$ (nM)	$\langle R_{nonspecific} \rangle$	$K_{d(nonspecific)}$ (nM)
H'(39)	4.9 \pm 0.1	0.54 \pm 0.02	0.7 \pm 0.1	2.6 \pm 0.1	35.7 \pm 4.2
H'(36)	5.5 \pm 0.1	0.44 \pm 0.04	0.6 \pm 0.1	2.2 \pm 0.3	24.7 \pm 6.8
H'(34)	6.3 \pm 0.1	0.38 \pm 0.04	0.7 \pm 0.1	1.8 \pm 0.3	36.8 \pm 11.3
H'(34)A	4.4 \pm 0.1	0.55 \pm 0.03	1.8 \pm 0.2	2.7 \pm 0.4	71.4 \pm 17.5
Control	NA	NA	NA	2.6 \pm 0.5	22.2 \pm 6.4

9. Average surface densities of 10 dsDNA spots and bound IHF at equilibrium

Table 4S. Average surface densities \pm SD ($\times 10^{12}$ cm⁻²) of 10 dsDNA spots and bound IHF at equilibrium for each DNA sequence.

	H'(39)	H'(36)	H'(34)	H'(34)A	Control
DNA surface density	1.94 \pm 0.03	1.75 \pm 0.03	2.05 \pm 0.03	1.39 \pm 0.03	1.64 \pm 0.05
IHF surface densities					
@ 1.25 nM	0.80 \pm 0.03	0.66 \pm 0.02	0.57 \pm 0.02	0.39 \pm 0.03	0.36 \pm 0.03
@ 2.5 nM	1.16 \pm 0.03	1.00 \pm 0.04	0.91 \pm 0.02	0.78 \pm 0.03	0.47 \pm 0.04
@ 5 nM	1.48 \pm 0.03	1.28 \pm 0.05	1.10 \pm 0.03	0.84 \pm 0.06	0.68 \pm 0.04
@ 10 nM	2.07 \pm 0.03	1.84 \pm 0.06	1.53 \pm 0.03	1.10 \pm 0.06	1.35 \pm 0.06
@ 20 nM	2.78 \pm 0.02	2.28 \pm 0.08	2.04 \pm 0.03	1.52 \pm 0.07	2.10 \pm 0.09
@ 40 nM	3.63 \pm 0.03	3.11 \pm 0.09	2.69 \pm 0.04	2.06 \pm 0.10	2.95 \pm 0.13

10. Effects of surface densities on the binding and conformational change of DNA

The IHF-to-DNA binding ratio results presented in this paper were obtained from the average surface densities of the DNA and IHF molecules of 10 DNA spots for each DNA sequence quantified by WLRS. We include the quantified results of the average surface densities of the DNA spots and subsequently bound IHF for each DNA sequence at equilibrium in Table 4S.

Previous studies have shown that surface densities of surface-immobilized DNA layers can affect the accessibility of the DNA molecules to molecules in solution and binding kinetics. For example, it is well known that the surface density of ssDNA molecules affects their hybridization efficiency with complementary strands^{10,11}. The DNA surface hybridization regimes and mechanisms have been studied extensively to optimize DNA microarrays for detecting target DNA sequences. Also, various optical, electrical, and mechanical techniques have been developed to characterize the surface density, conformation, or thickness of the DNA molecules immobilized on functionalized surfaces such as gold, quartz crystal, silicon, silicon dioxide or diamond^{12,3,13-21}. However, only a few publications report the effect of the surface density and conformation of surface-immobilized DNA on the binding of DNA and protein^{22,23}. We believe such study is important for optimizing the binding assay and obtaining accurate quantitative results. We thus conducted experiments to study the effect of DNA surface density on the binding of surface-immobilized dsDNA and IHF and binding induced conformational changes.

We examined the effect of DNA surface density on the measured average fluorophore height change, and the dissociation constants obtained from fitting the equilibrium isotherms. First, we prepared DNA microarrays with different DNA sequences spotted with solutions containing three different DNA concentrations (5 μM , 7.5 μM , and 15 μM) to prepare dsDNA spots of each sequence at approximately three different surface density groups: low density, medium density, and high density. These results are included in Tables 5S and 6S, and Figures 7S-10S below.

We observed that with increased DNA surface density, the dissociation constant of IHF specific binding to DNA, $K_{d(\text{specific})}$, increased, while the dissociation constant of IHF nonspecific binding to DNA, $K_{d(\text{nonspecific})}$, decreased. Also, the measured average fluorophore height change decreased as DNA surface density increased. These observations collectively suggest that specific binding of IHF to the DNA layer is inhibited while nonspecific binding of IHF to the DNA layer is enhanced as DNA surface density increases. However, the effects of DNA surface density on IHF binding for DNA sequence H' (39) were not as obvious as those for DNA sequences H'(34) and H'(36). Based on these observations of the effect of DNA surface density on the different binding parameters, we propose the interpretations below.

First, as shown in Figure 7S, the increase of $K_{d(\text{specific})}$ with DNA surface density suggests that specific binding of IHF to DNA is inhibited as DNA surface density increases. This could be because that the high-density DNA layers on the surface obstructed the accessibility of IHF to the specific binding sites on the surface-immobilized DNA molecules. This phenomenon resembles the macromolecular crowding effects in living cells, where DNA molecules are packaged tightly by various nucleoid associated proteins on the chromosome²⁴. The crowding of DNA molecules obstructs DNA-binding proteins from their specific binding sites, and thus affects their binding dissociation constants. This effect of DNA surface density is less observable for DNA sequence H'(39), whose specific binding site is further away from the surface and more accessible to the IHF molecules.

Further, as shown in Figure 8S, the average fluorophore height change decreased with increased DNA surface density, which suggests that dense DNA layer may increase the steric hindrance for specific DNA binding. This effect is again less observable for DNA sequence H'(39), whose specific binding site is further away from the surface and more accessible to the IHF molecules. Thus, both the reduced accessibility of the H' binding sites and the increased steric hindrance of the surface-immobilized

DNA layer could have inhibited the over all specific binding of IHF to the surface-immobilized DNA molecules, and lead to less specific binding, which is consistent with the reduced average IHF to DNA specific binding ratio, $\langle R_{specific} \rangle$. See Figure 9S.

It is also plausible that the average fluorophore height change decreases with increased DNA surface density is a result of decreased $\langle R_{specific} \rangle$ and ensemble averaging. However, the increase of DNA surface density also increases DNA orientation, which in turn could result in greater average fluorophore height change. Thus, DNA surface density can have two opposite effects on fluorophore height changes caused by DNA bending. We thus calculated the DNA bending angle to examine whether increased surface density caused steric hindrance and resulted in smaller DNA bending. The calculated bending angles are shown in Table 6S. As shown in Table 6S, the specific bending angle decreases as the surface density increases for all DNA sequences. Further, specific bending angle decreases as the binding location moves close to the surface of the substrate. These results show that binding site locations and surface densities of the DNA spots can affect the specific bending of dsDNA molecules caused by IHF binding, and need to be carefully examined and assessed.

Table 5S. Average surface densities \pm SD ($\times 10^{12}$ cm⁻²) of three groups of 10 DNA spots for each DNA sequence.

DNA sequence	H'(39)	H'(36)	H'(34)	H'(34)A	Control
Low Density	1.94 \pm 0.03	1.75 \pm 0.03	2.05 \pm 0.03	1.39 \pm 0.03	1.64 \pm 0.05
Medium Density	2.40 \pm 0.01	2.40 \pm 0.02	2.99 \pm 0.03	2.36 \pm 0.04	2.87 \pm 0.03
High Density	3.11 \pm 0.05	3.35 \pm 0.04	3.95 \pm 0.03	3.17 \pm 0.03	3.87 \pm 0.04

Table 6S. Average DNA bending angles \pm SD ($^{\circ}$) of three groups of DNA spots.

DNA sequence	H'(39)	H'(36)	H'(34)	H'(34)A
Low Density	162.4 \pm 11.3	153.4 \pm 15.1	150.6 \pm 12.1	124.2 \pm 26.2
Medium Density	159.4 \pm 15.3	142.5 \pm 8.7	126.1 \pm 20.3	122.1 \pm 28.9
High Density	151.8 \pm 11.6	134.7 \pm 16.9	129.2 \pm 20.6	113.8 \pm 28.2

On the other hand, the dissociation constant of nonspecific binding of IHF to DNA molecules, $K_{d(nonspecific)}$, generally decreased as DNA surface densities increases. See Figure 10S. This suggests that nonspecific binding of IHF to DNA was enhanced as DNA surface density increases. This is probably due to the reinforced negative surface potential of the DNA layer, which enhances electrostatic interactions between negatively charged DNA and positively charged proteins. The electrostatic interactions are mainly responsible for the nonspecific binding. Thus, nonspecific binding of IHF to the surface-immobilized DNA is enhanced as DNA surface density increases.

Based on the above observations, we selectively used the DNA spots with low surface densities to quantitatively evaluate the DNA conformational changes caused by IHF binding. The data and discussion presented in this section further demonstrate the advantages of our imaging biosensor system for optimizing and studying surface-based binding assays by enabling the examination of both surface density and conformational change.

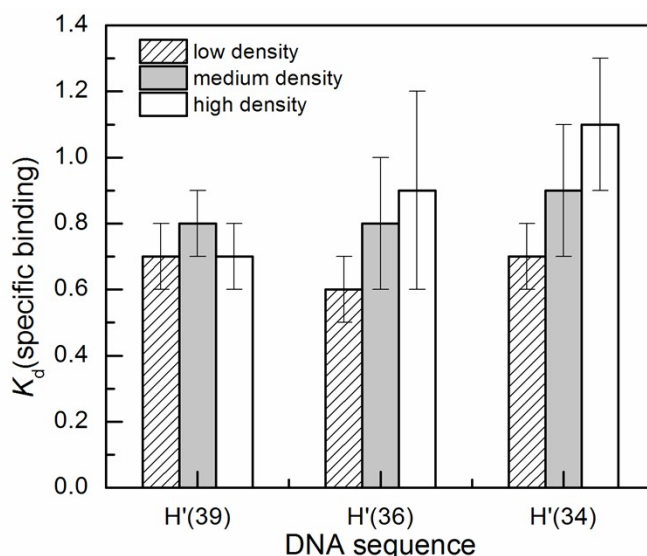


Figure 7S. The dissociation constants of IHF specific binding at different DNA surface densities.

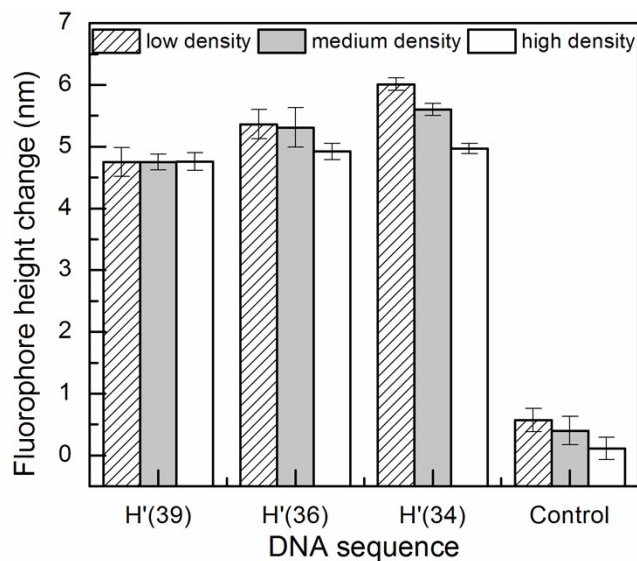


Figure 8S. Average fluorophore height changes at different DNA surface densities.

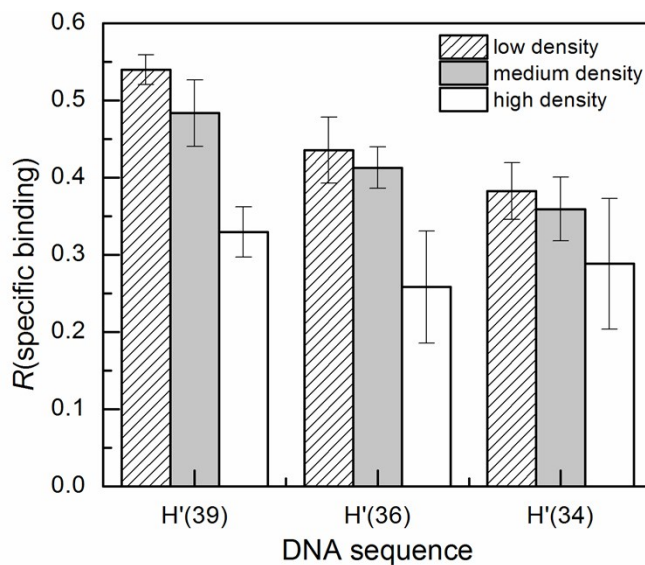


Figure 9S. IHF to DNA specific binding ratios at different DNA surface densities.

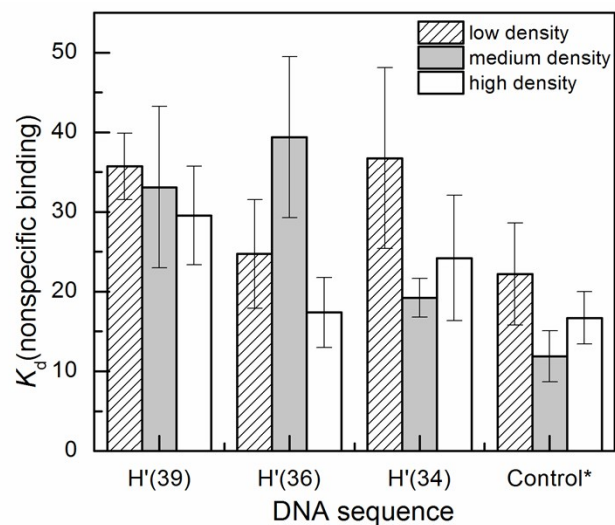


Figure 10S. Dissociation constants of IHF nonspecific binding to DNA at different DNA surface densities.

* $K_{d(\text{nonspecific})}$ for the Control sequence was obtained from fitting equilibrium results to the adapted Langmuir binding isotherm.

11. References

1. J. A. Holbrook, O. V. Tsodikov, R. M. Saecker, and M. T. Record Jr, *Journal of Molecular Biology*, 2001, **310**, 379–401.
2. G. M. Dhavan, D. M. Crothers, M. R. Chance, and M. Brenowitz, *Journal of Molecular Biology*, 2002, **315**, 1027–1037.
3. U. Rant, K. Arinaga, S. Fujita, N. Yokoyama, G. Abstreiter, and M. Tornow, *Langmuir*, 2004, **20**, 10086–10092.
4. U. Rant, K. Arinaga, M. Tornow, Y. W. Kim, R. R. Netz, S. Fujita, N. Yokoyama, and G. Abstreiter, *Biophysical Journal*, 2006, **90**, 3666–3671.
5. P. Spuhler, X. Zhang, M. Monroe, J. Greenspun, M. S. Ünlü, L. Sola, and M. Chiari, 2011, pp. 91–92.
6. X. Zhang, G. G. Daaboul, P. S. Spuhler, D. S. Freedman, A. Yurt, S. Ahn, O. Avci, and M. S. Ünlü, *Analyst*, 2014, **00**, 1–10.
7. A. R. Khokhlov, A. Y. Grosberg, and V. S. Pande, *Statistical Physics of Macromolecules (Polymers and Complex Materials)*, American Institute of Physics, 1994th edn. 1997.
8. P. A. Rice, S. Yang, K. Mizuuchi, and H. A. Nash, *Cell*, 1996, **87**, 1295–1306.
9. T. M. Squires, R. J. Messinger, and S. R. Manalis, *Nature Biotechnology*, 2008, **26**, 417–426.
10. P. Gong and R. Levicky, *Proceedings of the National Academy of Sciences*, 2008, **105**, 5301–5306.
11. D. Irving, P. Gong, and R. Levicky, *J. Phys. Chem. B*, 2010, **114**, 7631–7640.
12. L. Moiseev, M. S. Ünlü, A. K. Swan, B. B. Goldberg, and C. R. Cantor, *Proceedings of the National Academy of Sciences*, 2006, **103**, 2623–2628.
13. E. Mirmomtaz, M. Castronovo, C. Grunwald, F. Bano, D. Scaini, A. A. Ensafi, G. Scoles, and L. Casalis, *Nano Lett.*, 2008, **8**, 4134–4139.
14. N. E. Marotta, K. R. Beavers, and L. A. Bottomley, *Anal. Chem.*, 2013, **85**, 1440–1446.
15. G. Papadakis, A. Tsortos, F. Bender, E. E. Ferapontova, and E. Gizeli, *Anal. Chem.*, 2012, **84**, 1854–1861.
16. B. Rezek, D. Shin, H. Uetsuka, and C. E. Nebel, *phys. stat. sol. (a)*, 2007, **204**, 2888–2897.
17. K. Wang, C. Goyer, A. Anne, and C. Demaille, *J. Phys. Chem. B*, 2007, **111**, 6051–6058.
18. S. N. Patole, A. R. Pike, B. A. Connolly, B. R. Horrocks, and A. Houlton, *Langmuir*, 2003, **19**, 5457–5463.
19. D. Y. Petrovykh, H. Kimura-Suda, M. J. Tarlov, and L. J. Whitman, *Langmuir*, 2004, **20**, 429–440.
20. D. Y. Petrovykh, H. Kimura-Suda, L. J. Whitman, and M. J. Tarlov, *J. Am. Chem. Soc.*, 2003, **125**, 5219–5226.
21. A. Barhoumi, D. Zhang, and N. J. Halas, *J. Am. Chem. Soc.*, 2008, **130**, 14040–14041.
22. M. Castronovo, S. Radovic, C. Grunwald, L. Casalis, M. Morgante, and G. Scoles, *Nano Lett.*, 2008, **8**, 4140–4145.
23. P. S. Spuhler, J. Knezevic, A. Yalcin, Q. Bao, E. Pringsheim, P. Droge, U. Rant, and M. S. Ünlü, *Proceedings of the National Academy of Sciences*, 2010, **107**, 1397–1401.
24. H. Matsuda, G. G. Putzel, V. Backman, and I. Szleifer, *Biophysical Journal*, 2014, **106**, 1801–1810.